Shape evolution with increasing angular momentum in the ^{66}Ga nucleus

S. S. Bhattacharjee,* R. P. Singh, S. Muralithar, Indu Bala, and R. Garg
Inter University Accelerator Centre, Aruna Asaf Ali Marg, New Delhi 110067, India

S. Rajbanshi
Department of Physics, Dum Dum Motijheel College, Kolkata 700074, India

D. Singh
Centre for Applied Physics, Central University of Jharkhand, Brambe, Ranchi 835205, India

A. Dhal
Variable Energy Cyclotron Centre, Kolkata 700064, India

M. Kumar Raju
Nuclear Physics Department, Andhra University, Visakhapatnam 530003, India

S. Saha, J. Sethi, and R. Palit
Tata Institute of Fundamental Research, Mumbai 400005, India
(Received 4 April 2017; published 31 May 2017)

The high-spin nuclear structure of the odd-odd ^{66}Ga nucleus was probed using heavy-ion induced fusion-evaporation reaction. The de-exciting γ rays were detected by using the Indian National Gamma Array (INGA) consisting of high resolution Compton suppressed clover detectors. The level scheme of ^{66}Ga was extended up to an excitation energy (E_x) of ~10.6 MeV with spin parity of $21^{(+)}$. Two new quadrupole bandlike structures, one positive and one negative parity, based on the states having spin parity of $J^\pi = 11^+$ and 10^-, respectively, were found. The experimental energy levels are compared with calculations within the framework of shell model calculation using $jj44bpn$ effective interaction. The agreement between experiment and theory is good. The total Routhian surface calculations were performed to understand the shape of the ^{66}Ga nucleus associated with the configurations $\nu(g_{9/2})^3\,\nu(f_{5/2})^2\,\pi(g_{9/2})^1\,\pi(f_{5/2})^2$ and $\nu(g_{9/2})^2\,\nu(f_{5/2})^1\,\pi(g_{9/2})^1\,\pi(f_{5/2})^2$ assigned to the positive and negative parity bands, respectively. In the frequency domain $\omega = 0.20$–0.30 MeV, both the negative and positive parity quadrupole structures, favor prolate deformation whereas at $\omega = 0.50$ MeV there is a sudden change to noncollective oblate shape in both the bands.

DOI: 10.1103/PhysRevC.95.054330

I. INTRODUCTION

The odd-odd ^{66}Ga nucleus, with $Z = 31$ and $N = 35$, is located in between doubly magic spherical ^{56}Ni and deformed ^{76}Sr nuclei. Energy levels of the ^{56}Ni nucleus and its nearby neighbors exhibit single-particle excitations which have been explained well in the framework of spherical shell model calculations [1,2]. Low mass Sr and Kr isotopes along the $N = Z$ line, exhibit collective behavior which has strong dependence on the deformation parameters [1]. The neutron deficient Ga isotopes lie in between these two regions. Hence, they exhibit both single-particle as well as collective behavior (both prolate and oblate) in their energy levels. The valence protons and neutrons in the ^{66}Ga nucleus occupy $1p_{3/2}$ and $0f_{5/2}$ orbitals, respectively, outside the ^{56}Ni core. The ground-state spin parity of the odd-odd ^{66}Ga nucleus is 0^+ which was measured from decay study [3].

In case of nuclei with $N \sim Z$ and $A \sim 70$ regions, valence nucleons lie in fpg orbitals [4–6]. The high j intruder $0g_{9/2}$ orbital plays an important role in nuclear structure studies in this region. The increase of occupancy in the deformation driving $0g_{9/2}$ orbital increases the collectivity for nuclei in this mass region. In the $A \sim 60$ region as one goes away from N and $Z \sim 40$ shell closure a variety of structural phenomena have been observed and nuclear shape evolves from prolate to oblate with decreasing nucleon numbers [1]. For example, an oblate shape was predicted for the ground-state band in ^{68}Ge whereas an extremely soft triaxial deformation was predicted in ^{64}Ge [2]. Most of the nuclei in the N and $Z = 30$–42 region, four quasiparticle proton, and/or neutron alignment in $0g_{9/2}$ are found to drive the shape to lower deformation. The experimental results as well as total Routhian surface (TRS) calculations reflect that odd mass Ga ($A = 63$, 65) nuclei are moderately deformed ($\beta_2 \sim 0.25$) and γ soft at low rotational frequencies [1]. In the present investigation, we report a detailed investigation of the high spin states in the ^{66}Ga nucleus using heavy-ion induced fusion-evaporation reaction.

Most of the previous work on the level structure of the ^{66}Ga nucleus was based on experimental investigations using modest detector setups and light-ion beams. Decay of

*souphy85@gmail.com

electron capture and ^{64}Zn($\alpha, pn\gamma$), ^{63}Cu(α,$n\gamma$), ^{64}Zn(α,d), ^{66}Zn(p,$n\gamma$), ^{66}Zn(^{3}He,t) [7–13] reactions were used for these investigations. An isomeric state in the ^{66}Ga nucleus was studied by Filevich *et al.* [$E_x = 1441$ keV and $T_{1/2} = 57.3(14)$ ns] by using heavy-ion induced fusion-evaporation reaction [^{56}Fe(^{13}C,$2pn\gamma$)] [13,14]. The results of these measurements exhibit substantial uncertainties in spin-parity assignments, γ-ray angular distributions, and level lifetime measurements even at low excitation energies and spins. For example, spin parity of a 4162-keV level was assigned tentatively as (11) from the mixture of quadrupole and octupole characters of the de-exciting 1119-keV transition [13]. These observables play a major role in nuclear structure investigations and are expected to constrain the theoretical model calculations. Thus there is a need for detailed investigation and extension of the previous work using heavy-ion induced fusion-evaporation reaction to understand the high spin structure of ^{66}Ga.

The details of experimental data analysis are explained in Sec. II. Section III contains experimental results and outcomes, Sec. IV is composed of a theoretical description of the experimental findings, and the last section contains the conclusion.

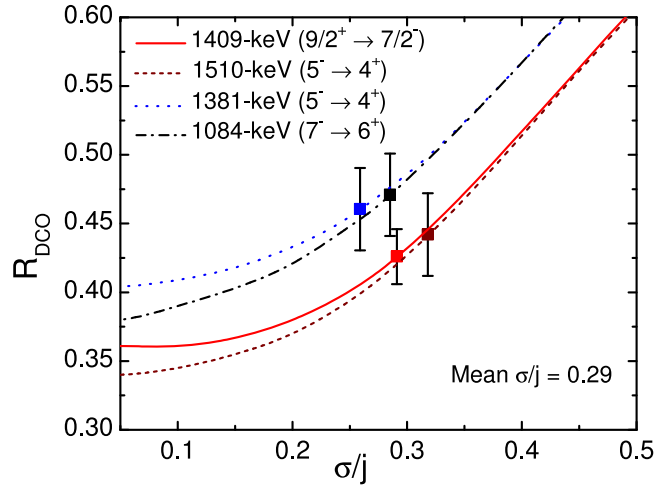

FIG. 1. Theoretical $R_{\rm DCO}$ values for different σ/j value of the reaction for the present experimental setup, calculated using the ANGCOR program. Experimental $R_{\rm DCO}$ ratios for the transitions of energy 1084-keV ($7^- \rightarrow 6^+$), 1409-keV ($9/2^+ \rightarrow 7/2^-$), 1510-keV ($5^- \rightarrow 4^+$), and 1381 ($5^- \rightarrow 4^+$)-keV transitions in ^{60}Ni, ^{61}Cu, ^{66}Ge, and ^{68}Ge nuclei, respectively. Mean value of $\sigma/j = 0.29$.

II. EXPERIMENTAL DETAILS AND DATA ANALYSIS

High spin states in ^{66}Ga were populated using the heavy-ion fusion evaporation reaction ^{56}Fe (^{12}C,pn) at a beam energy of 62 MeV. The ^{12}C beam was provided by Pelletron Linac Facility at Tata Institute of Fundamental Research (TIFR), Mumbai. The target was a thick natural iron. The de-exciting γ-ray transitions were detected by the Indian National Gamma Array (INGA) [15,16] which at the time of the experiment consisted of 15 Compton suppressed clover detectors arranged in six different angles [40°(2), 65°(2), 90°(4), 115°(2), 140°(2), and 157°(3)] with respect to the beam axis (number in parenthesis is the number of detectors at respective angles). The fast digital data acquisition system based on Pixie-16 modules from XIA LLC [17] was used for collecting the in-beam data. The data acquisition system is described in Ref. [15].

Energy and efficiency calibration of detectors was carried out using radioactive ^{152}Eu and ^{133}Ba sources, placed at the target position of the INGA setup. Time stamped data were sorted into different symmetric and angle-dependent E_γ-E_γ matrices using the MultipARameter time-stamped-based COincidence Search program (MARCOS) [15,18] and the matrices were analyzed using RADWARE [19,20] with a 100-ns coincidence time window. In total about 5.1 billion two- and higher-fold γ-γ coincident events were recorded in list mode.

Spin parity of the levels was determined from the measurement of directional correlation from oriented state (DCO) ratios [21,22], angular distribution from oriented nuclei (ADO) ratios [23], and linear polarization asymmetry measurements.

An extensively used technique for information on dominant multipolarity of the γ transition is determination of the DCO ratio and was carried out in the present work. The DCO ratio for a gamma transition (γ_1) at an angle θ_1 with respect to another transition (γ_2) at an angle θ_2 is defined as

$$R_{\rm DCO} = \frac{I^{\theta_1}_{\gamma_1}(\text{at } \theta_1 \text{ gated by } \gamma_2 \text{ at } \theta_2)}{I^{\theta_2}_{\gamma_1}(\text{at } \theta_2 \text{ gated by } \gamma_2 \text{ at } \theta_1)}, \quad (1)$$

where $I^{\theta_1}_{\gamma_1}$ [$I^{\theta_2}_{\gamma_1}$] is the intensity of γ_1 at an angle θ_1 [θ_2], and when the energy gate is set on γ_2 at an angle θ_2 [θ_1]. In the present investigation, detectors at $\theta_1 = 157^\circ$ and $\theta_2 = 90^\circ$ with respect to the beam direction were used to determine $R_{\rm DCO}$ values for multipolarity assignments of the γ -ray transitions. Theoretical $R_{\rm DCO}$ values for the observed γ transitions were calculated using the code ANGCOR [24]. Theoretically, for a stretched transition, the $R_{\rm DCO}$ value should be close to unity if the gating transition is the same multipolarity as that of the observed transition. DCO ratios for a stretched dipole (quadrupole) transition gated by a pure quadrupole (dipole) transition are ∼0.5(2.0). $R_{\rm DCO}$ value depends on detector angles, mixing ratio (δ), and width of substate population (σ/j) in the reaction.

Therefore, to evaluate the mixing ratio (δ) for a mixed transition from the measured DCO ratio, it is essential to estimate the value of σ/j for the present fusion evaporation reaction. For this purpose several electric dipole ($E1$) transitions of known multipolarity having energy 1084 ($7^- \rightarrow 6^+$)-, 1409 ($9/2^+ \rightarrow 7/2^-$)-, 1510 ($5^- \rightarrow 4^+$; mixing $\delta(M2/E1) = -0.02$)-, and 1381 ($5^- \rightarrow 4^+$; mixing $\delta(M2/E1) = +0.04$)-keV transitions in ^{60}Ni, ^{61}Cu, ^{66}Ge, and ^{68}Ge nuclei, respectively [13], populated in the same reaction, were selected. DCO ratios were evaluated using the stretched pure $E2$ transition as the gating transition so that the gating and the observed (analyzed) transitions were of different multipolarities. DCO ratios were compared with the values calculated using ANGCOR with spin alignment (σ/j) being varied as a parameter, to check for the best compliance. The calculated DCO ratios for these transitions, with different values of σ/j are shown in Fig. 1.

It can be seen from the figure (Fig. 1) that experimental DCO ratios for the 1084-, 1409-, 1510-, and 1381-keV γ transitions were reproduced with the width of the substate population (σ/j) as 0.29, 0.29, 0.32, and 0.26, respectively. To calculate the mixing ratios (δ) for the transitions in ^{66}Ga, we have thus adopted $\sigma/j = 0.29$ which is the weighted average of the aforesaid values.

ADO ratio (R_θ) for a γ transition (γ_1) was obtained from the relation,

$$R_\theta = \frac{I_{\gamma_1}(\text{Measured at } \theta_1 = 157^\circ; \text{Gated by all})}{I_{\gamma_1}(\text{Measured at } \theta_2 = 90^\circ; \text{Gated by all})}. \quad (2)$$

Here I_{γ_1} [Measured at θ_1 (θ_2) = 157° (90°); gated by all] corresponds to γ-ray coincidence intensity observed by detectors at an angle θ_1 (θ_2) by setting gates on the detectors at all angles. For this purpose, two asymmetric matrices were constructed. First one consisted of events with γ rays detected at 157° on one axis and coincident events from all angles were placed on the other axis. The other matrix was similar to the first one except for the fact that the γ rays detected at 90° were placed on one axis instead of 157°. Typical R_θ values were ∼0.9 (1.5) for the stretched dipole (quadrupole) γ-ray transitions whereas it deviates from these values for the mixed transitions.

Clover detectors at 90° of the INGA were used for measurement of linear polarization (P) which provide useful information regarding assignment of the electromagnetic character of the γ transitions. Two asymmetric E_γ-E_γ matrices were constructed with horizontally ($N_\parallel$) or vertically ($N_\perp$) scattered γ rays with respect to the reaction plane (contains both the beam axis and the emission direction of the γ ray) at 90° detectors on one axis and the coincident γ-ray events from all other detectors on the second axis. The linear polarization (P) of a γ-ray transition is expressed as $P = \Delta/Q$, where Q and Δ are polarization sensitivity and polarization asymmetry, respectively. The linear polarization asymmetry ratio [25–29] can be expressed as

$$\Delta(E_\gamma) = \frac{a(E_\gamma)N_\perp - N_\parallel}{a(E_\gamma)N_\perp + N_\parallel}. \quad (3)$$

Here, the asymmetry correction factor [$a(E_\gamma) = N_\parallel(\text{unpolarized})/N_\perp(\text{unpolarized})$] represents the geometrical (instrumental) asymmetry of the detection system. It was determined by using unpolarized radioactive ^{152}Eu and ^{133}Ba sources and its value was found to be close to unity [1.01(1)] for the present experimental setup (shown in Fig. 2). The value of $Q(E_\gamma)$ was dependent on γ-ray energy of interest and was parametrized as

$$Q(E_\gamma) = (CE_\gamma + D)Q_0(E_\gamma), \quad (4)$$

where

$$Q_0(E_\gamma) = \frac{(\alpha + 1)}{(\alpha^2 + \alpha + 1)} \quad (5)$$

was the sensitivity for an ideal Compton polarimeter, with

$$\alpha = \frac{E_\gamma(\text{MeV})}{0.511}. \quad (6)$$

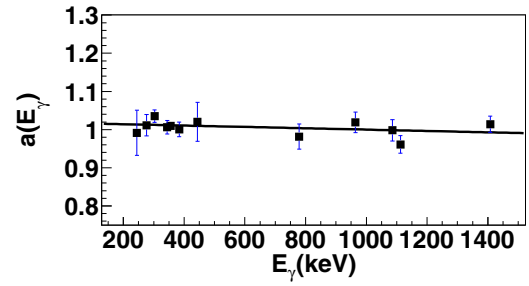

FIG. 2. Plot of asymmetry factor a with energy for a 90° clover detector (with respect to beam direction) in the present setup. The solid line shows a linear fit to the data points.

Polarization sensitivity was calculated for γ transitions of previously known multipolarity and mixing ratios as given in Refs. [29–31]. Figure 3 depicts variation of polarization sensitivity of 90° detectors with γ-ray transitions observed in the present experiment. The least-squares fitting of experimental polarization sensitivity $Q(E_\gamma)$ with Eq. (4) gives C = 1.52(978) × 10^{-5} [keV^{-1}] and D = 0.59(5).

Measured P values for γ-ray transitions in nuclei populated in the present experiment are shown in Fig. 4. These experimental results were compared with the theoretical polarization values which were obtained as outlined in Refs. [32,33] considering σ/J (width of the m-state distribution) =0.29. Positive, negative, and near-zero P values are expected for the γ-ray transitions of electric, magnetic, and mixed character, respectively. The calculated polarization values for several transitions in ^{66}Ga along with the reference transitions are in qualitative agreement with the experimental results, as shown in Fig. 4.

III. EXPERIMENTAL RESULTS

Several nuclei were populated in the present reaction as depicted in the total projection spectrum of the E_γ-E_γ symmetric matrix (Fig. 5). The original experiment was ^{150}Nd as a target and ^{12}C as a projectile at $E_{\text{lab}} = 62$ MeV. However, in the present experiment a part of the beam was falling on the natural iron target frame resulting in the population of several nuclei in the A ∼ 60 region. The total projection spectrum of the symmetric E_γ-E_γ matrix shows that along

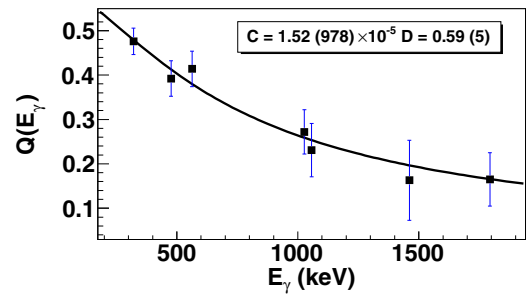

FIG. 3. Plot of the polarization sensitivity with energy for different γ-ray transitions observed in the present experiment. The solid curve is obtained by fitting the data with Eq. (4).

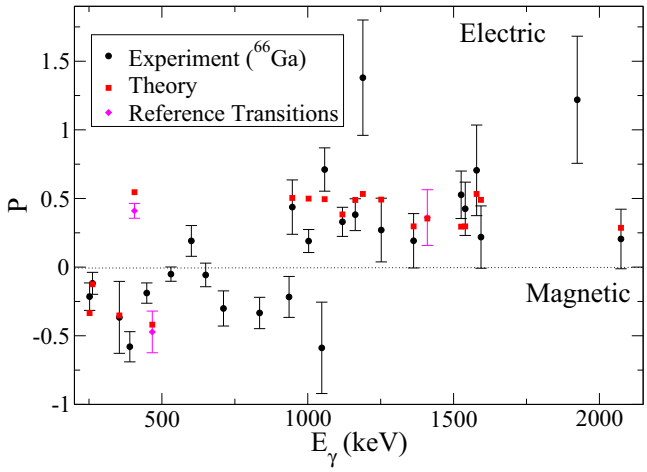

FIG. 4. Plot of the experimental and theoretical value of polarization for different γ-ray transitions observed in the present experiment.

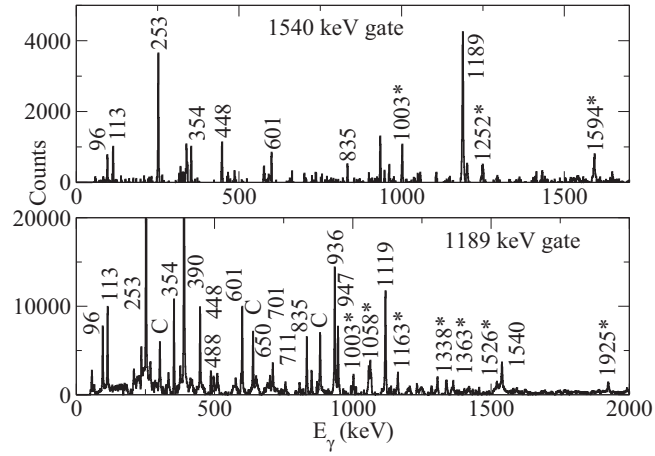

FIG. 6. Gated spectrum on 1189-keV ($9^+ \rightarrow 7^+$) and 1540-keV ($10^- \rightarrow 9^+$) transitions in ^{66}Ga. Transitions belonging to the ^{66}Ga nucleus are labeled with the respective energies and new transitions are indicated by asterisks (*) while contaminant peaks are identified with C.

with strongly populated channels, the ^{66}Ga nucleus is also populated with a reasonable cross section (∼8% of the total cross section). Single gated spectra created by the gates of energies 1189 keV ($9^+ \rightarrow 7^+$) and 1540 keV ($10^- \rightarrow 9^+$) show almost all previously observed transitions along with the observation of several new transitions, marked by asterisks, in ^{66}Ga (Fig. 6).

The proposed partial level scheme of ^{66}Ga, obtained from the present experiment (Fig. 7), was established using γ-γ coincidence relationships, relative intensity (I_γ), DCO ratio ($R_{\rm DCO}$), R_θ, and polarization measurements. Most of the γ transitions, previously observed by Morand *et al.* [8], were confirmed in the present investigation except low energy γ-ray transitions whose energies were below low energy threshold. The 44-keV ($1^+ \rightarrow 0^+$) and 22-keV ($(2)^+ \rightarrow 1^+$) γ-ray transitions which decay from the 44-keV ($J^\pi = 1^+$) and 66-keV ($J^\pi = (2)^+$) levels were not observed in the present work. The 44-keV ($1^+ \rightarrow 0^+$) transition was previously observed by Bolotin and his co-workers [7] and they had assigned it as $M1$ in nature from comparison of the corrected internal conversion coefficient with single particle estimates. They also observed 382-, 537-, and 706-keV excited levels which decay to the ground state 0^+ of the ^{66}Ga nucleus. Spin parity of these levels have been assigned as 1^+ from the isobaric-spin forbiddenness for Fermi transitions [7]. In the present experiment the fact that all three levels were not observed may be because of the preferential population of the high-spin states in the heavy-ion induced reaction used in the present investigation [33]. The level scheme was extended up to an excitation energy ≈10.6 MeV and spin parity of $21^{(+)}$. A total of 17 new excited levels have been placed in the proposed level scheme of ^{66}Ga, which show complex and irregular structure at low spin. Intensities of the γ transitions above the 44-keV [$J^\pi = 1^+$] excited state in ^{66}Ga were determined from the symmetrized E_γ-E_γ matrix and normalized with intensity of the 253-keV ($4^+ \rightarrow 3^+$) γ transition. The γ-ray transition energies (E_γ), I_γ, $R_{\rm DCO}$, R_θ, P, Δ, and spin parities of the levels of ^{66}Ga are given in Table I.

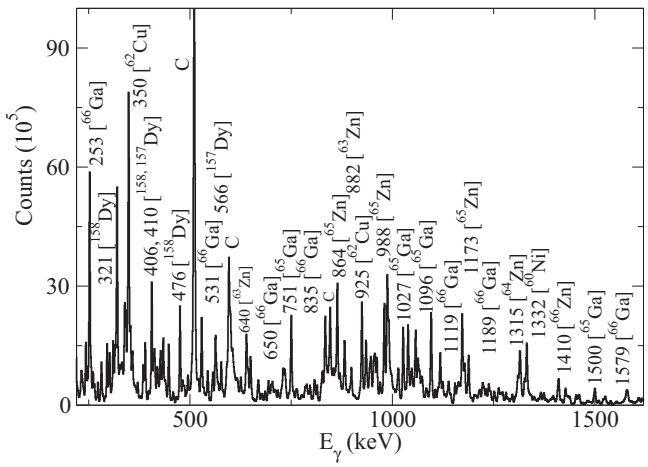

FIG. 5. Total projection spectrum of E_γ-E_γ matrix from ^{12}C + ^{56}Fe reaction at $E_{\rm lab} = 62$ MeV shows γ rays of nuclei populated in the present reaction. Contaminant peaks are identified with C. Nuclei in $A \sim 150$ region were populated from the reaction of ^{12}C beam with the ^{150}Nd target.

In previous work by Morand *et al.*, a 1119-keV quadrupole ($L = 2$) transition with considerable amount of $L = 3$ (octupole) mixing, which decays from the 4162-keV level, with mixing ratio $\delta = 0.16\,(20)$ was reported [8]. Consequently, spin parity of the 4162-keV excited state remained tentative. This was indicative of structural changes at this spin in this nucleus. In fact, a bandlike structure consisting of regular γ energies 947, 1058, 1163, 1439, and 1799 keV, based on the 4162-keV excited level, was observed. To explore the intrinsic structure of this band, it is important to have firm assignment of spin and parity of this excited state. Hence, in the present experiment, the electromagnetic character of the 1119-keV γ transition, de-exciting from the 4162-keV excited level was extracted.

Measured values of $R_{\rm DCO}$ and R_θ for the 1119-keV transition are 1.09(3) and 1.34(2), respectively, indicating

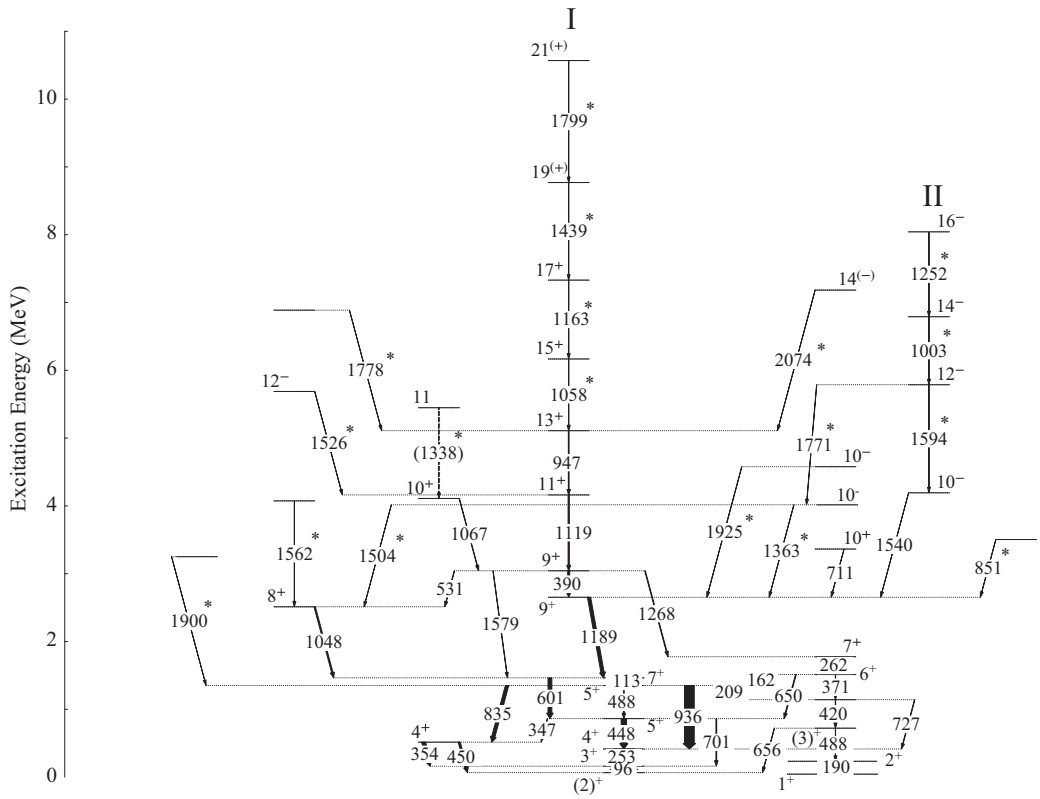

FIG. 7. Proposed partial level scheme of ^{66}Ga nucleus obtained from the present work. Transitions marked with asterisks (*) are newly observed in the current measurement. Widths of the arrows are proportional to the transition intensities. Tentatively identified transition is indicated by dotted line.

a dominant quadrupole nature in agreement to previous assignments. This value of $R_{\rm DCO}$ can be theoretically calculated by considering 1119-keV transition for possible combinations of different multipole, viz. a dipole with considerable amount of quadrupole admixture [$M1 + E2$ or $E1 + M2; \delta = +0.48(3)$] or a quadrupole with a small mixing [$\delta = +0.10(3)$] of multipole order $L = 3$ (octupole) or else an octupole with hexadecapole ($L = 4$) admixing [$\delta = -0.15(4)$], as shown in Fig. 8. The Weisskopf estimate of the level lifetime of the state, depopulated by the 1119-keV transition, is ~fs for a mixed $M1 + E2$ or $E1 + M2$ transition and ~ns in case of $E2 + M3$ or $M2 + E3$ transition de-exciting the state. This estimate gives ~μs level lifetime if the de-exciting transition has an $E3 + M4$ or $M3 + E4$ character. Corresponding experimental half-life of the level is <2 ns [13] that excludes the possibility of the 1119-keV γ-ray transition being of $E3 + M4$ or $M3 + E4$ in nature and consequently a possible mixing of the $L = 2$ ($E2$ or $M2$) with the $L = 1$ ($M1$ or $E1$) character or with a small octupole ($E3$ or $M3$) component (10%) to the quadrupole ($L = 2$) nature can exist in the 1119-keV transition.

To get a better idea about multipolarity of the transition of interest, 1119 keV, we calculated the theoretical polarization (P_{th}) value by considering these possibilities and the values are

$$P_{\rm th}\,[E1/M2; \delta = +0.48(3)] = -0.05(2),$$
$$P_{\rm th}\,[M1/E2; \delta = +0.48(3)] = +0.05(2),$$
$$P_{\rm th}\,[E2/M3; \delta = +0.10(3)] = +0.43(3),$$

and

$$P_{\rm th}\,[M2/E3; \delta = +0.10(3)] = -0.43(3).$$

Measured polarization asymmetry (Δ) and corresponding linear polarization ($P = \Delta/Q$) values for the 1119-keV transition are +0.08(2)and +0.33(11), respectively, which clearly indicate that it must have mixed $M3/E2$ character. Therefore, these spectroscopy measurements unambiguously establish $M3/E2$ character of the 1119-keV γ-ray transition, having mixing ratio of +0.10(3), in compliance with the previous studies on this nucleus.

To further resolve the nature of the 1119-keV γ transition we performed the angular distribution measurements. Normalized experimental intensity for the transition of interest at a different angle [$W(\theta)$] with respect to the beam axis was fitted with the distribution function,

$$W(\theta) = A_0[1 + a_2 P_2(\cos\theta) + a_4 P_4(\cos\theta)]\,,$$

where a_2 and a_4 are the angular distribution coefficients [34,35]. Figure 9 shows measured angular distribution along with the fitted values for the 1119-keV γ transition. The fitted values of the a_2 and a_4 coefficients are +0.51(4) and −0.16(6), respectively, in compliance with a mixed $E2 + M3$ character.

To determine mixing ratio from the measured a_2 and a_4 coefficients, we calculated these theoretically considering the partial degree of alignment as described by Yamazaki *et al.* [30] and by Der Mateosian and Sunyar [31]. In case of partial

TABLE I. Energy (E_γ), relative intensity (I_γ), $R_{\rm DCO}$, R_θ, linear polarization (P), and assignment of the γ transitions in ^{66}Ga measured in the present reaction are presented.

E_i(keV)	E_γ(keV)	E_f(keV)	I_γ(%)	J_i^π	J_f^π	$R_{\rm DCO}$[a]	R_θ	Δ	$P_{\rm expt}$	Assignment
162	96.2(1)	66	122.76(330)	3^+	$(2)^+$	0.70(3)	0.95(3)			$(M1+E2)$[b]
234	189.9(1)	44	1.57(50)	2^+	1^+	0.82(6)	1.11(4)			$M1+E2$[b]
415	252.8(3)	162	100.00(280)	4^+	3^+	0.41(1)	1.04(1)	−0.11(5)	−0.21(10)	$M1+E2$
516	353.6(2)	162	19.04(100)	4^+	3^+	0.46(1)	0.98(1)	−0.17(12)	−0.36(26)	$M1$
	450.2(1)	66		4^+	$(2)^+$					
722	488.0(2)	234	1.07(40)	$(3)^+$	2^+					
	656.1(3)	66	1.63(60)	$(3)^+$	$(2)^+$					$M1$[b]
863	448.0(1)	415	26.40(160)	5^+	4^+	0.45(2)	0.64(2)	−0.08(3)	−0.19(7)	$M1+E2$
	347.1(2)	516	0.48(40)	5^+	4^+					
	700.6(9)	162	3.72(150)	5^+	3^+	0.98(7)	1.32(15)			Q
1142	419.9(3)	722	2.10(30)		$(3)^+$					
	727.5(3)	415	2.10(40)		4^+					
1351	209.0(4)	1142	1.09(30)	5^+		0.71(17)	1.18(4)			$D+Q$
	487.6(1)	863	3.99(80)	5^+	5^+	1.17(7)	1.27(3)			$(D+Q)$
	834.6(2)	516	15.91(190)	5^+	4^+	0.44(2)	0.75(2)	−0.10(3)	−0.33(11)	$M1$
	935.7(1)	415	47.96(70)	5^+	4^+	0.47(2)	0.75(1)	−0.06(4)	−0.21(15)	$M1$
1464	113.2(2)	1351	18.73(50)	7^+	5^+	1.01(4)	1.74(4)			$E2$[b]
	600.9(3)	863	18.66(240)	7^+	5^+	1.15(17)	1.37(3)	+0.07(4)	0.19(11)	$E2+M3$
1513	162.5(8)	1351	3.76(70)	6^+	5^+					$(D(+Q))$[b]
	371.4(1)	1142	1.72(50)	6^+						
	650.1(1)	863	3.61(50)	6^+	5^+		0.85(2)	−0.02(3)	−0.05(8)	$M1+E2$
1775	261.6(2)	1513	5.20(60)	7^+	6^+		1.00(3)	−0.06(4)	−0.12(8)	$M1+E2$
2512	1048.1(2)	1464	6.50(30)	8^+	7^+	0.98(3)	1.80(6)	−0.15(8)	−0.59(33)	$M1+E2$
2653	1188.9(3)	1464	15.73(40)	9^+	7^+	0.96(4)	1.51(2)	+0.32(7)	1.38(42)	$E2$
3043	390.0(1)	2653	9.64(40)	9^+	9^+	1.36(3)	1.83(2)	−0.26(4)	−0.58(11)	$M1+E2$
	531.2(2)	2512	1.77(20)	9^+	8^+	0.87(6)	0.91(2)	−0.02(2)	−0.05(5)	$M1+E2$
	1268.4(2)	1775	3.13(50)	9^+	7^+		1.37(3)			Q
	1579.2(3)	1464	1.44(30)	9^+	7^+	1.03(6)	1.51(3)	+0.13(5)	0.71(33)	$E2$
3251	1899.5(3)	1351	0.43(10)		5^+					
3364	710.8(2)	2653	1.03(20)	10^+	9^+	0.54(4)	1.14(5)	−0.10(4)	−0.30(13)	$M1+E2$
3504	851.4(5)	2653	0.98(20)		9^+					
4016	1363.5(2)	2653	0.77(10)	10^-	9^+	0.56(18)	1.01(4)	+0.04(4)	0.19(20)	$E1$
	1504.2(5)	2512	0.52(10)	10^-	8^+					
4074	1562.0(6)	2512	1.45(40)		8^+					
4110	1066.8(3)	3043	1.89(50)	10^+	9^+	0.37(2)	0.55(8)	−0.12(21)	−0.48(84)	$M1+E2$
4162	1118.7(4)	3043	5.99(120)	11^+	9^+	1.09(3)	1.34(2)	+0.08(2)	0.33(11)	$E2+M3$
4193	1540.0(1)	2653	0.63(20)	10^-	9^+	0.71(5)	0.64(2)	+0.08(3)	0.43(19)	$E1$
4578	1924.5(3)	2653	1.13(30)	10^-	9^+	0.54(5)	1.01(5)	+0.19(4)	1.22(46)	$E1$
5109	947.0(2)	4162	3.52(40)	13^+	11^+	1.25(4)	1.43(4)	+0.12(5)	0.44(20)	$E2$
5448	1338.3(7)	4110	1.35(30)	11	10^+	0.83(4)	1.16(1)			$D+Q$
5688	1526.3(4)	4162	0.98(60)	12^-	11^+		0.79(2)	+0.10(2)	0.53(17)	$E1$
5787	1593.7(3)	4193	0.50(20)	12^-	10^-	0.96(9)	1.58(7)	+0.04(4)	0.22(23)	$E2$
	1770.5(4)	4016	0.93(60)	12^-	10^-	1.38(54)	1.78(40)			Q
6167	1058.0(2)	5109	1.83(20)	15^+	13^+	0.91(6)	1.54(7)	+0.18(2)	0.71(16)	$E2$
6790	1003.2(2)	5787	1.49(30)	14^-	12^-	1.07(27)	1.29(9)	+0.05(2)	0.19(8)	$E2$
6887	1778.2(4)	5109	0.82(10)		13^+					
7183	2074.0(20)	5109	0.75(20)	$14^{(-)}$	13^+	0.85(23)	1.02(2)	+0.03(3)	0.21(22)	$(E1)$
8042	1252.1(3)	6790	0.94(20)	16^-	14^-	0.85(2)	1.42(3)	+0.06(5)	0.27(23)	$E2$
7330	1163.5(5)	6167	1.00(30)	17^+	15^+	0.93(13)	1.83(27)	+0.09(2)	0.38(12)	$E2$
8769	1439.4(7)	7330	0.30(10)	$19^{(+)}$	17^+	1.03(33)	1.37(32)			Q
10568	1798.7(3)	8769	0.11(10)	$21^{(+)}$	$19^{(+)}$	0.85(19)	1.35(34)			Q

[a]From quadrupole gate.
[b]Adopted from NNDC.

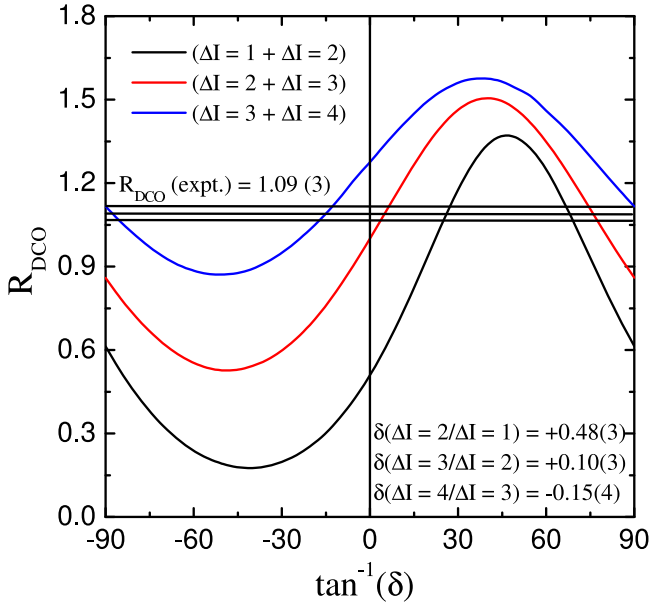

FIG. 8. Plot of theoretical R_{DCO} values for different δI mixing represented by the solid blue, red, and black colored lines. Experimental R_{DCO} for 1119-keV transition are represented by the solid black horizontal lines.

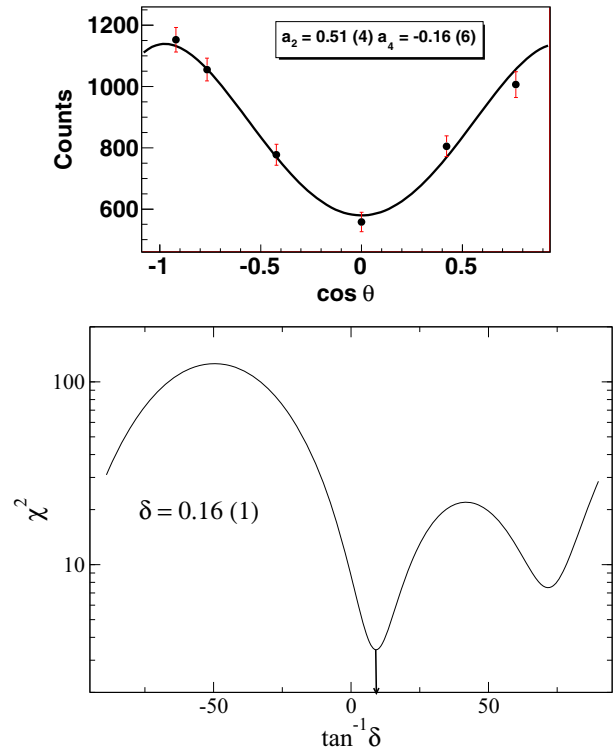

FIG. 9. Angular distribution fit for the 1119-keV ($11^+ \rightarrow 9^+$) transition in the ^{66}Ga nucleus and the corresponding χ^2 analysis for obtaining the mixing ratio.

alignment, angular distribution coefficients are expressed as

$$a_k = \alpha_k A_k^{\max}.$$

Here, $A_k^{\max}$ is the angular distribution coefficient for complete alignment and it is defined as [30,31]

$$A_k^{\max}(J_i L_1 L_2 J_f) = \frac{f_k(J_f L_1 L_1 J_i) + 2\delta f_k(J_f L_1 L_2 J_i) + \delta^2 f_k(J_f L_2 L_2 J_i)}{1+\delta^2},$$

where L_1 and L_2 are angular momenta of γ ray with $L_2 = L_1 + 1$ and δ is the mixing ratio of the γ ray. The values of f coefficients are tabulated in Refs. [30,31] for different J_i values. The attenuation coefficient α_k depends on J and distribution of the nuclear state over its m substates [30,31]. The mixing ratio (δ) was extracted from the χ^2 minimization of the experimental angular distribution coefficients (a_2 and a_4) with the theoretically calculated values (considering $\sigma/j = 0.29$) as shown in Fig. 9 and the value was found to be +0.16(1). This value is in close agreement with the value obtained from analysis of the R_{DCO} and polarization asymmetry results. Thus, a spin parity of 11^+ was assigned to the state depopulated by the 1119-keV transition.

The R_{DCO}, R_θ, and linear polarization (P) values of the 947-keV transition confirmed its $E2$ nature, leading to assign a spin parity of 13^+ to the 5109-keV excited state which is populated by 1778-, 2074-, and 1058-keV transitions. The measured values of the R_{DCO}, R_θ, and linear polarization (P) for the 2074- and 1058-keV transitions establish their ($E1$) and $E2$ character and both the states were assigned spin parity of $14^{(-)}$ and 15^+, respectively. We could not perform these measurements for the 1778-keV transition owing to its weak intensity. A 1526-keV transition was observed in coincidence with 1119-keV transition and remains unobserved in the 947-keV gated spectrum. Thus, the 1526-keV transition was placed above the 11^+ state and parallel to the 947-keV transition.

Two bandlike structures have been observed in the high energy spectrum of ^{66}Ga and are labeled as I and II in Fig. 7.

A. Band I

Above the 11^+ level, a cascade consisting of the 947-, 1058-, 1163-, 1439-, and 1799-keV transitions, was observed in band I (Fig. 7). Measured R_{DCO}, R_θ, and P values for the 947-, 1058-, and 1163-keV transitions indicate these as stretched $E2$ transitions. For the 1439- and 1799-keV γ-ray transitions, their P values could not be measured because of the weak nature of the transitions. However, measured values of R_{DCO} and R_θ for these two transitions give sufficient justification for identifying them to be stretched $E2$ transitions. Hence, corresponding states were assigned as $19^{(+)}$ and $21^{(+)}$, respectively.

B. Band II

The γ-ray transitions of energies 1363 and 1540 keV have been observed in coincidence with 1189-keV γ ray but is absent in gated spectra by 390- and 1119-keV transitions. Hence, 1363- and 1540-keV transitions are placed above the 2653-keV [9^+] level and parallel to 390-keV γ-ray transition. Measured values of R_{DCO}, R_θ, and P for the 1363- and 1540-keV γ-ray transitions showed $E1$ character. Spin parity of both states, through which they depopulate, were assigned 10^-. In the gated spectrum of the 1540-keV transition (Fig. 6),

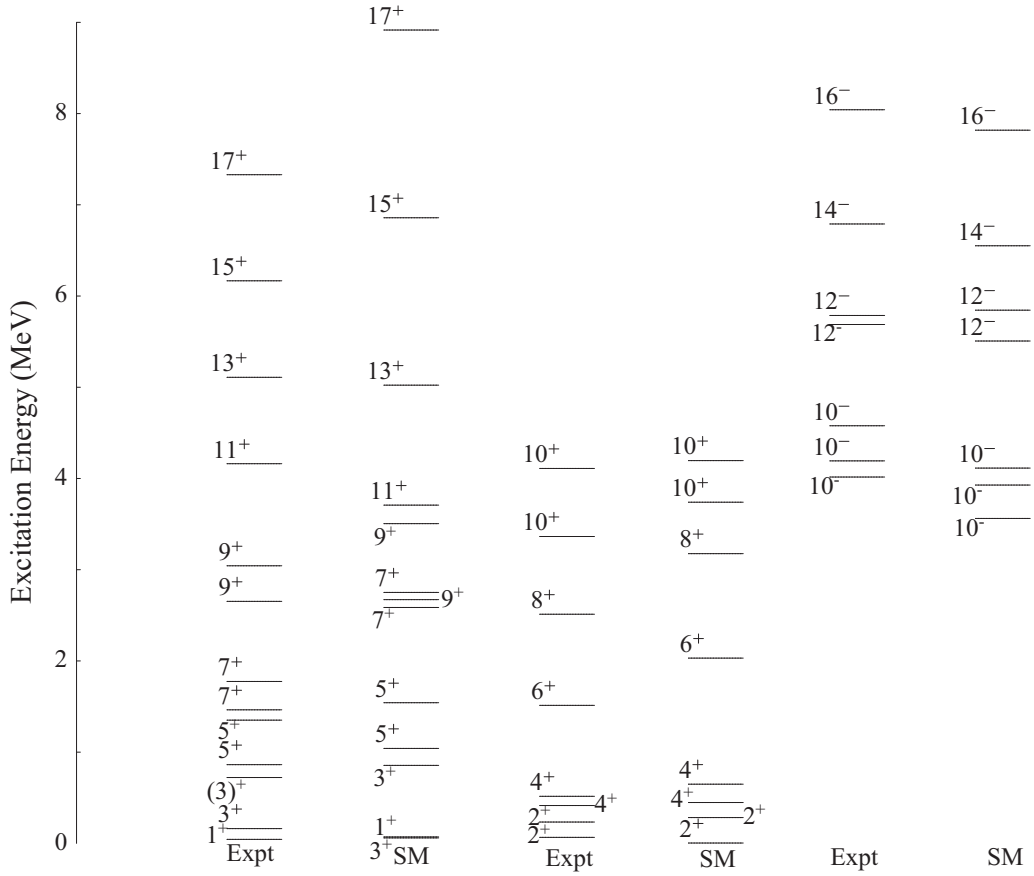

FIG. 10. Comparison of energy levels of ^{66}Ga observed in the present data (denoted by Expt) with shell model calculations using $jj44bpn$ [36] effective interaction (denoted by SM) for both positive as well as negative parity states.

a cascade of 1594-, 1003-, and 1252-keV γ-ray transitions were observed. $R_{\rm DCO}$, R_θ, and P values of the 1594-, 1003-, and 1252-keV γ transitions confirmed their $E2$ character and corresponding states were assigned spin parity of 12^-, 14^-, and 16^-, respectively.

The 1003- and 1252-keV γ-ray transitions were also observed in the gated spectrum of the 1363-keV transition. This required a $\Delta I = 2$, $E2$ connection between 12^- and 10^- states. The gated spectrum of the 1363-keV transition had a peak of 1771 keV which fitted the energy gap between the 12^- and the 10^- levels. However, measurement of P was not performed because of its weak nature but values of $R_{\rm DCO}$ and R_θ confirmed the $\Delta I = 2$ character.

IV. DISCUSSION

Proposed partial level scheme of ^{66}Ga, as shown in Fig. 7, it is an irregular and complex structure at low excitation energies whereas bandlike structures were observed at high excitation energies. In the sections below we discuss the observed level structure in the framework of spherical shell model and TRS calculations.

A. Shell model calculations

Shell model calculations were carried out to understand present experimental observations by using updated interaction and proper truncation schemes. Calculations were performed by using NUSHELLX @ MSU [37] code and model space comprising $0f_{5/2}$, $1p_{3/2}$, $1p_{1/2}$, and $0g_{9/2}$ orbitals, which is known as the $jj44pn$ model space. The adopted interaction is $jj44bpn$ which was used successfully in this mass region [36,38]. Three valence protons and seven valence neutrons lie outside the doubly magic ^{56}Ni core. Particle excitations from the core could not be considered in the present calculations. The calculations within the aforesaid interaction and model space which includes the fpg orbitals, reproduces both of the positive and negative parity states without any adjustment of single particle energies.

Comparison of the shell model calculations with the experimental energy levels are presented in Fig. 10. It was observed from Fig. 10 that both of the positive and negative parity energy states are well reproduced. There is large deviation ($E_{\rm SM} - E_{\rm expt} \geqslant 1$ MeV) between the shell model and the experimentally observed energy levels for the positive parity 7_1^+, 7_2^+, and 17_1^+ states. In case of 7_1^+ state discrepancy from the presence of a long-lived isomeric state [$T_{1/2} = 57.3$ (14) ns] [13] whereas the level lifetime of 7_2^+ is not known which also may be an isomeric state [39]. The discrepancy in the 17_1^+ level is from development of collectivity at this spin in ^{66}Ga. In fact, quadrupole band structure I was observed in the proposed partial level scheme above the 11_1^+ state in this nucleus. The gradually increasing deviation between the shell model prediction and experimental energy levels

TABLE II. Average particle occupancies of positive parity states in ^{66}Ga from shell model calculations.

J^π	E_{expt} (keV)	E_{SM} (keV)	Particles	$0f_{5/2}$	$1p_{3/2}$	$1p_{1/2}$	$0g_{9/2}$
1_1^+	44	71	p	0.52	1.77	0.48	0.21
			n	2.46	2.98	0.95	0.59
2_1^+	66	4	p	0.94	1.39	0.44	0.22
			n	2.85	2.86	0.59	0.68
3_1^+	162	60	p	0.66	1.66	0.43	0.23
			n	2.78	2.96	0.62	0.61
2_2^+	234	283	p	0.79	1.54	0.44	0.21
			n	2.65	2.80	0.74	0.79
4_1^+	415	448	p	0.99	1.41	0.32	0.25
			n	2.89	2.77	0.59	0.73
4_2^+	516	649	p	0.70	1.66	0.39	0.24
			n	2.70	2.90	0.68	0.70
3_5^+	722	855	p	0.91	1.46	0.42	0.20
			n	2.56	2.65	0.82	0.95
5_1^+	863	1041	p	1.07	1.38	0.30	0.23
			n	2.78	2.80	0.62	0.78
5_2^+	1351	1542	p	0.87	1.47	0.44	0.19
			n	2.70	2.85	0.70	0.73
7_1^+	1464	2586	p	0.89	0.81	0.48	0.80
			n	2.75	2.23	0.53	1.47
6_1^+	1513	2031	p	1.03	1.43	0.31	0.21
			n	2.95	2.77	0.62	0.64
7_2^+	1775	2751	p	1.07	1.45	0.29	0.17
			n	2.69	2.83	0.69	0.77
8_1^+	2512	3176	p	1.23	0.80	0.37	0.58
			n	2.51	2.00	0.58	1.89
9_1^+	2653	2672	p	0.90	0.73	0.41	0.95
			n	2.65	2.40	0.59	1.33
9_2^+	3043	3505	p	0.99	0.88	0.33	0.78
			n	2.63	2.21	0.71	1.43
10_1^+	3364	3740	p	1.15	1.07	0.35	0.41
			n	2.62	2.00	0.54	1.82
10_2^+	4110	4196	p	1.15	0.87	0.31	0.65
			n	2.51	2.19	0.63	1.65
11_1^+	4162	3708	p	0.88	0.69	0.47	0.94
			n	2.88	2.29	0.50	1.31
13_1^+	5109	5023	p	0.93	0.73	0.34	0.98
			n	2.81	2.35	0.57	1.25
15_1^+	6167	6858	p	0.97	0.73	0.29	0.99
			n	2.84	2.38	0.57	1.19
17_1^+	7330	8916	p	1.05	0.85	0.07	1.01
			n	2.53	2.58	0.73	1.14

throughout band structure I, as shown in Table II, indicates the development of collectivity along the positive parity band.

Average particle occupancies of positive and negative parity levels are listed in Tables II and III. From this table it is clear that the contribution of the neutron $0g_{9/2}$ orbital suddenly increased for the 7_1^+ level and it attains maximum value at the 8_1^+ level. The contribution of the neutron $0g_{9/2}$ orbital gradually falls up to the 17_1^+ level. In negative parity levels the neutron $0g_{9/2}$ orbital contribution is more compared to the proton. The neutron $0g_{9/2}$ contribution sharply jumps in case of 14_1^- and 16_1^- levels. Similarly, the proton contribution in the

TABLE III. Average particle occupancies of negative parity states in ^{66}Ga from shell model calculations.

J^π	E_{expt} (keV)	E_{SM} (keV)	Particles	$0f_{5/2}$	$1p_{3/2}$	$1p_{1/2}$	$0g_{9/2}$
10_1^-	4016	3562	p	1.19	1.23	0.40	0.16
			n	2.52	2.62	0.60	1.24
10_2^-	4193	3928	p	1.49	0.98	0.38	0.14
			n	2.72	2.42	0.54	1.30
10_3^-	4578	4114	p	1.19	1.31	0.31	0.16
			n	2.52	2.56	0.69	1.22
12_1^-	5688	5507	p	1.29	1.24	0.30	0.15
			n	2.43	2.63	0.69	1.23
12_2^-	5787	5845	p	1.32	0.88	0.39	0.38
			n	2.58	2.34	0.55	1.51
14_1^-	6790	6551	p	1.06	0.51	0.39	1.02
			n	2.81	1.68	0.44	2.04
16_1^-	8042	7818	p	1.03	0.55	0.38	1.02
			n	2.81	1.66	0.47	2.04

$0g_{9/2}$ orbital suddenly increases in 14_1^- and 16_1^- levels (listed in Table III). This shows that with increasing spin, particles are more likely to occupy deformation driving $0g_{9/2}$ orbital, promoted from the $1p_{3/2}$ orbital in case of negative parity band II.

B. Cranking and TRS calculations

In the transitional nucleus ^{66}Ga, the occupation of the $g_{9/2}$ orbital by protons as well as neutrons are expected to cause a variety of structural effects. These structural features arise from the Coriolis interactions between the protons and neutrons. The presence of the protons and neutrons in the $g_{9/2}$ orbitals prompted our expectation of the occurrence of shape coexistence and/or shape evolution in the ^{66}Ga nucleus.

Above the 11^+ level of the positive parity part of the level scheme, a quadrupole band structure is observed. Similar bandlike structures were observed in neighboring ^{63,65,68}Ga and ^{65}Zn nuclei [1,6,40]. In the previous study of ^{66}Ga by Morand *et al.*, the $\pi g_{9/2} \otimes \nu g_{9/2}$ configuration was assigned to 9^+, 3043-keV excited state. To explore the intrinsic structure of band I, we plotted the quasiparticle alignment (i_x) and the experimental Routhians (e') against the rotational frequency (ω), as shown in Fig. 11. The quasiparticle Routhian energy (e') and aligned angular momentum (i_x) are obtained by subtracting the reference from their absolute values, to account for their relative nature, as

$$e'(\omega) = E'(\omega) - E_{\mathrm{ref}}(\omega), \tag{7}$$

and

$$i(\omega) = I_x(\omega) - I_{x,\mathrm{ref}}(\omega), \tag{8}$$

respectively.

Absolute values of aligned quasiparticle angular momentum [$I_x(\omega)$] and Routhian [$E'(\omega)$] are expressed as

$$I_x = \sqrt{I(I+1) - K^2}, \tag{9}$$

and

$$E'(\omega) = \tfrac{1}{2}[E(I+1) + E(I-1)] - \hbar\omega I_x(I), \tag{10}$$

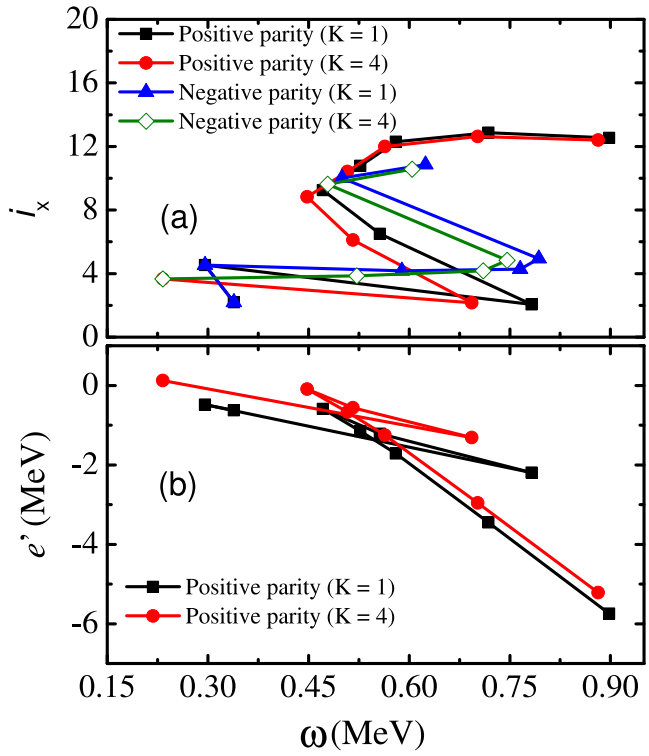

FIG. 11. Variation of experimental quasiparticle (a) aligned angular momentum and (b) Routhian for positive and negative parity band structures (band I and band II) in ^{66}Ga with frequency. Harris parameters used for the calculation are $J_0 = 6.0\hbar^2$ MeV^{-1} and $J_1 = 3.5\hbar^4$ MeV^{-3} [40].

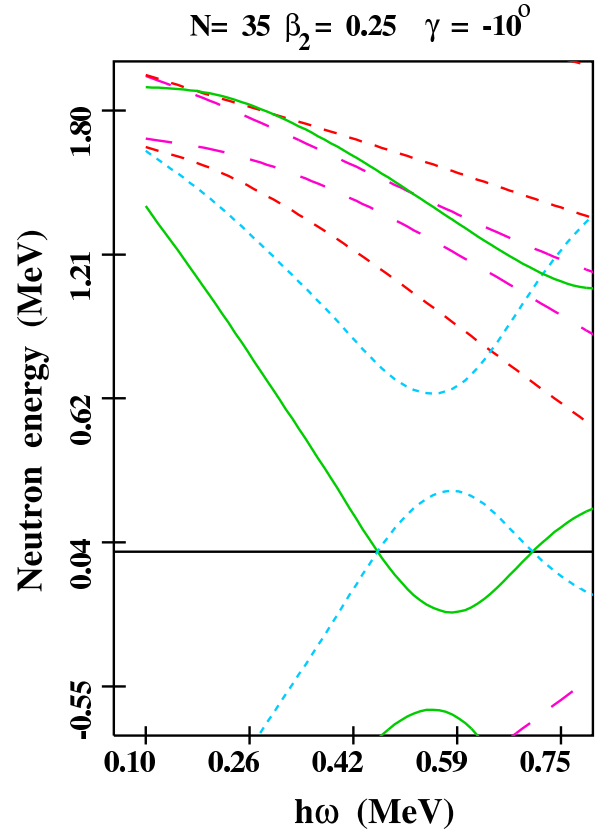

FIG. 12. Calculated quasineutron energy levels for $N = 35$ corresponding to the ^{66}Ga nucleus. Positive parity, positive, and negative signature, and negative parity, positive, and negative signature orbitals are denoted by green, blue, red, and magenta colors, respectively.

respectively. Here, I_x is the x component (rotational component) of the total angular momentum. The variable K refers to the projection of total angular momentum on the symmetry axis. The reference alignment angular momentum $[I_{x,\mathrm{ref}}(\omega)]$ and energy reference $[E_{\mathrm{ref}}(\omega)]$ are calculated using the following relations:

$$I_{x,\mathrm{ref}}(\omega) = (J_0 + \omega^2 J_1)\omega, \tag{11}$$

and

$$E_{\mathrm{ref}}(\omega) = -\frac{1}{2}\omega^2 J_0 - \frac{1}{4}\omega^4 J_1 + \frac{\hbar^2}{8J_0}, \tag{12}$$

where J_0 and J_1 are the Harris parameters. In the present case of ^{66}Ga, the Harris parameters used were $J_0 = 6.0\hbar^2$ MeV^{-1} and $J_1 = 3.5\hbar^4$ MeV^{-3} for the calculations [40].

It is evident from the quasiparticle alignment (i_x) vs ω and the experimental Routhians (e′) against the rotational frequency (ω) plots, as shown in Fig. 11, that there is a total gain in alignment of ∼8$\hbar$ at a frequency of ∼0.60 MeV for the positive parity band structure, band I. The quasiparticle aligned angular momentum was calculated for the two values of the projection of total angular momentum on the symmetry axis, $K = 1$ and 4, as K is not well defined in the low and medium spin states in ^{66}Ga. However, both the calculations reproduce similar alignment (i_x) and quasiparticle crossing at similar rotational frequencies (ω). Such alignment may be from second crossing of the $g_{9/2}$ orbital of the proton and/or neutron as the first crossing is blocked in ^{66}Ga. To understand the observed crossing we have calculated neutron and proton quasiparticle energies against rotational frequency (ω) at typical values of the deformation parameters $\beta_2 = 0.25$, $\beta_4 = 0.02$, and $\gamma = -10^\circ$ as shown in Figs. 12 and 13. The calculations show that the neutron quasiparticle crossing for the $g_{9/2}$ orbital occurs at rotational energy ($\hbar\omega$) of ∼0.60 MeV while the proton quasipaticle crosses at a rotational energy of ∼0.80 MeV. Therefore, the observed experimental crossing or alignment at a rotational energy of ∼0.60 MeV may be from the second crossing of the $g_{9/2}$ neutron orbital for the band I. The second crossing for the neutron is predicted to be at ∼0.80 MeV. However, this may change because it is quite sensitive to pairing strength. Therefore, the positive parity quadrupole band structure may be from coupling of four and or six aligned quasiparticles with the two-quasiparticle $(\pi g_{9/2} \otimes \nu g_{9/2})$ configuration assigned to the 9^+ level. This is consistent with the large gain in alignment (∼8$\hbar$) observed at $\hbar\omega \sim 0.60$ MeV. Such large gain in the aligned angular momentum was observed in ^{63,65,68}Ga and ^{65}Zn and was explained in terms of the alignment of a pair of the $g_{9/2}$ neutron quasiparticles. Therefore, the configuration $\nu(g_{9/2})^3\,\nu(f_{5/2})^2\,\pi(g_{9/2})^1\,\pi(f_{5/2})^2$ was designated to the positive parity band structure band I in ^{66}Ga. This configuration is similar to the assigned configuration of the positive parity quadrupole band based on the 9^+ state in ^{63}Ga. The maximum

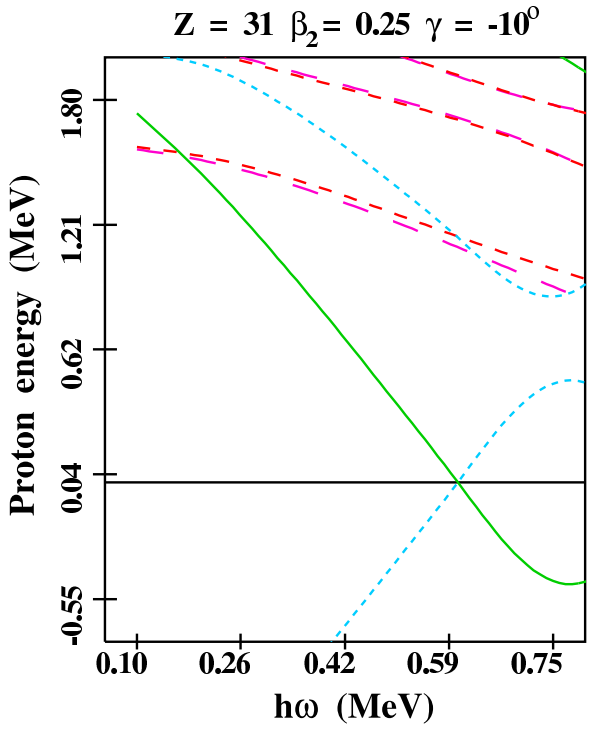

FIG. 13. Calculated quasiproton energy levels for $Z = 31$ corresponding to the ^{66}Ga nucleus. Positive parity, positive and negative signature and negative parity positive and negative signature orbitals are denoted by green, blue, red, and magenta colors, respectively.

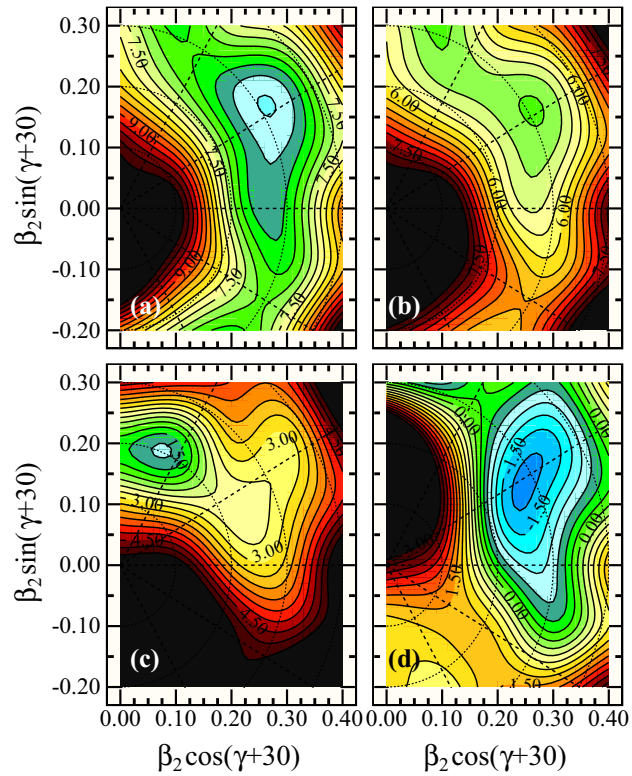

FIG. 14. Contour plots of the TRS calculations for the $\nu(g_{9/2})^3\,\nu(f_{5/2})^2\,\pi(g_{9/2})^1\,\pi(f_{5/2})^2$ configuration of the positive parity band structure in ^{66}Ga. The rotational frequency ($\hbar\omega$) for the calculations are (a) 0.200, (b) 0.300, (c) 0.500, and (d) 0.900 MeV. The energy difference between two contours is 0.250 MeV.

spin that can be generated from this configuration is $23\hbar$ which is close to the observed $21^{(+)}$, 10 568-keV state of this band structure.

The negative parity states in ^{66}Ga can be generated from the presence of the unpaired particle in the f or p orbital. However, for the generation of high spin states, it is energetically favorable to occupy the $g_{9/2}$ orbital compared to the fp orbital. Such an alignment is manifested by the large alignment followed by a strong backbending in the experimental spectra. The observed negative parity states above the 4193-keV, 10^- level may be from the coupling of an odd number of quasiparticles in the f or p orbital with the $g_{9/2}$ orbital to generate the angular momentum of the states. For the negative parity, the aligned angular momentum (i_x) shows a gain of $6\hbar$ at the rotational frequency ($\hbar\omega$) of 0.60 MeV (Fig. 11). As it is evident from the calculated proton and neutron quasiparticle energies such an alignment is from the crossing of the neutrons in the $g_{9/2}$ orbital not for the protons in the $g_{9/2}$ orbital, as shown in the Figs. 12 and 13, respectively. For this reason, the $\nu(g_{9/2})^2\,\nu(f_{5/2})^1\,\pi(g_{9/2})^1\,\pi(f_{5/2})^2$ configuration gives a maximum spin of $19\hbar$, and was adopted for the negative parity quadrupole bandlike structure in ^{66}Ga. This is in close agreement to the observed highest spin of $16\hbar$ in this band.

The shape evolution in this nucleus was studied theoretically by calculating the total Routhian surfaces (TRS) [41,42] at different rotational frequencies (ω). The total Routhian contains the macroscopic liquid drop energy of the nucleus, shell correction, and the pairing energy. The single-particle energies are obtained from a Woods-Saxon potential, and the pairing includes a monopole and a double-stretched quadrupole interaction [41]. The Routhian is minimized with respect to the deformation parameters β_2, β_4, and γ.

To understand the shape of the ^{66}Ga nucleus associated with the configurations $\nu(g_{9/2})^3\,\nu(f_{5/2})^2\,\pi(g_{9/2})^1\,\pi(f_{5/2})^2$ and $\nu(g_{9/2})^2\,\nu(f_{5/2})^1\,\pi(g_{9/2})^1\,\pi(f_{5/2})^2$ assigned to the positive parity (band I) and negative parity (band II), respectively, the total Routhian surface (TRS) calculations [41,42] have been performed. The TRS calculations for positive and negative parity bands have been performed with negative ($\alpha = 1$) and positive ($\alpha = 0$) signatures, respectively, in compliance with the experimentally observed spins. The contour plots of the TRS calculations of the above mentioned configurations for the positive and negative parity structures are presented in Figs. 14 and 15. The total Routhian surface (TRS) is calculated at each frequency ω in the β_2 plane with minimization on β_4. As observed in Figs. 14 and 15, at low frequencies with $\omega = 0.20$–0.30 MeV, both the negative and positive parity states favor prolate deformation ($\gamma \sim 0^\circ$). However, at $\omega \sim 0.50$ MeV, there is a sudden transition to noncollective oblate shape ($\gamma \sim 55^\circ$ for both the positive and negative parity structures) as the most favored one. At higher rotational frequencies, the prolate shape becomes energetically favored for both the parities [Figs. 14(d) and 15(d)]. Such transition can be associated with the rotation alignment of a pair of $g_{9/2}$ protons. The second crossing of the neutron quasiparticles

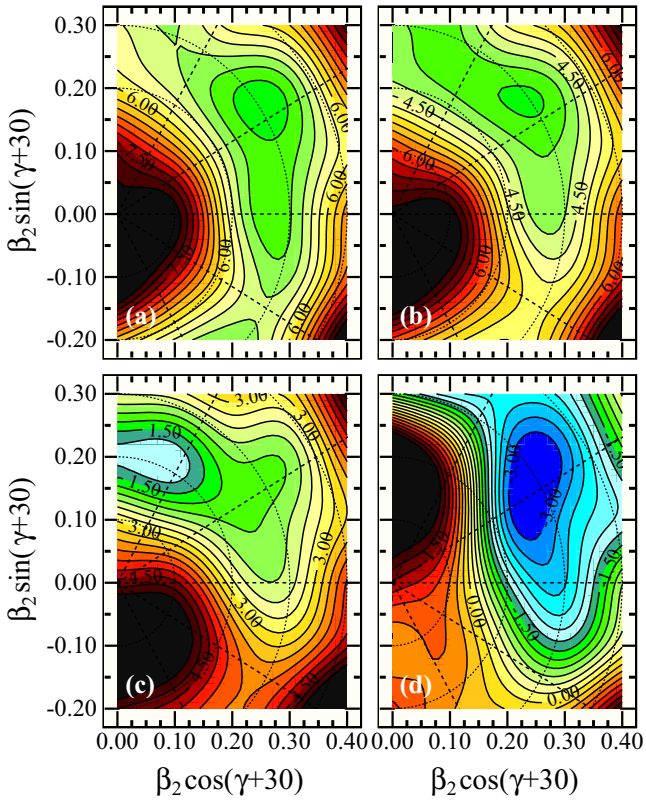

FIG. 15. Contour plots of the TRS calculations for the $\nu(g_{9/2})^2\,\nu(f_{5/2})^1\,\pi(g_{9/2})^1\,\pi(f_{5/2})^2$ configuration of the negative parity structure in ^{66}Ga. The rotational frequency ($\hbar\omega$) for the calculations are (a) 0.200, (b) 0.300, (c) 0.500, and (d) 0.900 MeV. The energy difference between two contours is 0.250 MeV.

in the $g_{9/2}$ neutron orbitals was observed explicitly at the rotational frequency $\hbar\omega \sim 0.60$ MeV as shown in Fig. 11. Such crossing was not observed in the proton quasiparticle energy levels in this frequency region as can be seen in Fig. 13.

V. CONCLUSIONS

The level structure of the ^{66}Ga nucleus was studied by using the heavy-ion induced fusion-evaporation reaction, and a large array of Compton suppressed clover detectors (INGA) was used to detect the de-exciting γ-ray transitions. The level scheme was extended up to 10.6-MeV excitation energy on the basis of γ-γ coincidence measurements. Seventeen new transitions were observed and placed in the level scheme of ^{66}Ga. The spin-parity assignments have been done by conventional $R_{\rm DCO}$, R_θ, and linear polarization measurements. The observed level structure was well explained by spherical shell model calculations using NUSHELLX@MSU [37] code without any adjustment to the single-particle energies. Deviation between shell model calculated energy levels and experimental results in 7_1^+, 7_2^+, and 17_1^+ levels were of the order of 1 MeV or more. The 7_1^+ state was a long-lived isomeric state and the shell model calculation could not explain this feature whereas the level lifetime of the 7_2^+ state still remains unknown which may also be an isomeric state [39]. The discrepancy in the 17_1^+ level may be from the development of collectivity in this nucleus. However, the discrepancy of $\sim$1 MeV with respect to experimentally observed energy levels might indicate the limitation of the Hamiltonian and omission of important excitation from the ^{56}Ni core.

To interpret the deformation characteristics in the ^{66}Ga nucleus TRS calculations were performed. The shape of the ^{66}Ga nucleus was interpreted with the configurations $\nu(g_{9/2})^3\,\nu(f_{5/2})^2\,\pi(g_{9/2})^1\,\pi(f_{5/2})^2$ and $\nu(g_{9/2})^2\,\nu(f_{5/2})^1\,\pi(g_{9/2})^1\,\pi(f_{5/2})^2$ for the positive and negative parity bands, respectively. At low frequency domain ($\omega =$ 0.20–0.30 MeV) both positive and negative parity states exhibit prolate deformation whereas at $\omega \sim 0.50$ MeV, a sudden transition to the noncollective oblate shape was observed in both parity states.

ACKNOWLEDGMENTS

We thank the staff of BARC-TIFR Pelletron Linac Facility for its excellent support during the experiment. The help and co-operation of members of the INGA collaboration in setting up the array is acknowledged. We thank B. S. Naidu and S. Jadhav (TIFR) for their help during the experiment. Discussion with Prof. S. C. Pancholi during the preparation of the manuscript is gratefully acknowledged. S.S.B. would like to acknowledge financial assistance from the Inter University Accelerator Centre (IUAC), India. The INGA Project was partially supported by the Department of Science and Technology (DST), Government of India (Grant No. IR/S2/PF-03/2003-I).

[1] M. Weiszflog, G. de Angelis, A. Axelsson, D. Bazzacco, F. Becker, M. D. Poli, J. Eberth, C. Fahlander, A. Gadea, S. Lunardi *et al.*, Eur. Phys. J. A **11**, 25 (2001).

[2] E. A. Stefanova, I. Stefanescu, G. de Angelis, D. Curien, J. Eberth, E. Farnea, A. Gadea, G. Gersch, A. Jungclaus, K. P. Lieb *et al.*, Phys. Rev. C **67**, 054319 (2003).

[3] H. Bakhru and I. M. Ladenbauer-Bellis, Phys. Rev. **184**, 1142 (1969).

[4] A. J. Nichols, R. Wadsworth, M. A. Bentley, P. J. Davies, J. Henderson, D. G. Jenkins, I. Paterson, H. Iwasaki, A. Lemasson, V. M. Bader *et al.*, Phys. Rev. C **91**, 014319 (2015).

[5] I. Dankó, D. Sohler, Z. Dombrádi, S. Brant, V. Krstić, J. Cederkäll, M. Lipoglavšek, M. Palacz, J. Persson, A. Atac *et al.*, Phys. Rev. C **59**, 1956 (1999).

[6] A. K. Singh, G. Gangopadhyay, D. Banerjee, R. Bhattacharya, R. K. Bhowmik, S. Muralithar, R. P. Singh, A. Goswami, S. Bhattacharya, B. Dasmahapatra *et al.*, Eur. Phys. J. A **9**, 197 (2000).

[7] H. H. Bolotin and D. A. McClure, Phys. Rev. **180**, 987 (1969).

[8] C. Morand, M. Agard, J. F. Bruandet, A. Dauchy, A. Giorni, F. Glasser, and T. U. Chan, Nucl. Phy. A **308**, 103 (1978).

[9] C. C. Lu, M. S. Zisman, and B. G. Harvey, Phys. Rev. **186**, 1086 (1969).
[10] J. Timár, T. X. Quang, T. Fényes, Z. Dombrádi, A. Krasznahorkay, J. Kumpulainen, R. Julin, S. Brant, V. Paar, and L. Šimičić, Nucl. Phys. A **573**, 61 (1994).
[11] M. R. Najam, W. F. Davidson, W. M. Zuk, L. E. Carlson, and M. A. Awal, Nucl. Phys. A **173**, 577 (1971).
[12] R. A. Hinrichs, R. Sherr, G. M. Crawley, and I. Proctor, Phys. Rev. Lett. **25**, 829 (1970).
[13] http://www.nndc.bnl.gov.
[14] A. Filevich, A. Ceballos, M. A. J. Mariscotti, P. Thieberger, and E. D. Mateosian, Nucl. Phys. A **295**, 513 (1978).
[15] R. Palit, S. Saha, J. Sethi, T. Trivedi, S. Sharma, B. S. Naidu, S. Jadhav, R. Donthi, P. B. Chavan, H. Tan *et al.*, Nucl. Instrum. Methods Phys. Res., Sect. A **680**, 90 (2012).
[16] R. Palit, S. Saha, J. Sethi, T. Trivedi, B. S. Naidu, P. B. Chavan, R. Donthi, and S. Jadhav, J. Phys. Conf. Proc. **420**, 012159 (2013).
[17] H. Tan *et al.*, in *Nuclear Science Symposium Conference Record 2008* (IEEE, Washington, DC, 2008), p. 3196.
[18] S. Saha, R. Palit, J. Sethi, T. Trivedi, P. C. Srivastava, S. Kumar, B. S. Naidu, R. Donthi, S. Jadhav, D. C. Biswas *et al.*, Phys. Rev. C **86**, 034315 (2012).
[19] D. C. Radford, Nucl. Instrum. Methods Phys. Res., Sect. A **361**, 297 (1995).
[20] D. C. Radford, Nucl. Instrum. Methods Phys. Res., Sect. A **361**, 306 (1995).
[21] A. Krämer-Flecken, T. Morek, R. M. Lieder, W. Gast, G. Hebbinghaus, H. M. Jäger, and W. Urban, Nucl. Instrum. Methods Phys. Res., Sect. A **275**, 333 (1989).
[22] M. K. Kabadiyski, K. P. Lieb, and D. Rudolph, Nucl. Phys. **563**, 301 (1993).
[23] M. Piiparinen, A. Atac, J. Blomqvist, G. B. Hagemann, B. Herskind, R. Julin, S. Juutinen, A. Lampinen, J. Nyberg, G. Sletten *et al.*, Nucl. Phys. **605**, 191 (1996).
[24] E. S. Macias, W. D. Ruhter, D. C. Camp, and R. G. Lanier, Comput. Phys. Commun. **11**, 75 (1976).
[25] K. Starosta, T. Morek, C. Droste, S. G. Rohoziński, J. Srebrny, A. Wierzchucka, M. Bergström, B. Herskind, E. Melby, T. Czosnyka *et al.*, Nucl. Instrum. Methods Phys. Res., Sect. A **423**, 16 (1999).
[26] C. Droste, S. G. Rohoziński, K. Starosta, T. Morek, J. Srebrny, and P. Magierski, Nucl. Instrum. Methods Phys. Res., Sect. A **378**, 518 (1996).
[27] J. K. Deng, W. C. Ma, J. H. Hamilton, A. V. Ramayya, J. Rikovska, N. J. Stone, W. L. Croft, R. B. Piercey, J. C. Morgan, P. F. Mantica *et al.*, Nucl. Instrum. Methods Phys. Res., Sect. A **317**, 242 (1992).
[28] P. M. Jones, L. Wei, F. A. Beck, P. A. Butler, T. Byrski, G. Duchêne, G. de. France, F. Hannachi, G. D. Jones, and B. Kharraja, Nucl. Instrum. Methods Phys. Res., Sect. A **362**, 556 (1995).
[29] R. Palit, H. C. Jain, P. K. Joshi, S. Nagaraj, B. V. T. Rao, S. N. Chintalapudi, and S. S. Ghugre, Pramana **54**, 347 (2000).
[30] T. Yamazaki, Nucl. Data A **3**, 1 (1967).
[31] E. D. Mateosian and A. W. Sunyar, At. Nucl. Data **13**, 391 (1974).
[32] R. Chakrabarti, S. Mukhopadhyay, Krishichayan, A. Chakraborty, A. Ghosh, S. Ray, S. S. Ghugre, A. K. Sinha, L. Chaturvedi, A. Y. Deo *et al.*, Phys. Rev. C **80**, 034326 (2009).
[33] S. S. Bhattacharjee, R. Bhattacharjee, R. Chakrabarti, R. Raut, S. S. Ghugre, A. K. Sinha, T. Trivedi, L. Chaturvedi, S. Saha, J. Sethi *et al.*, Phys. Rev. C **89**, 024324 (2014).
[34] L. C. Biedenharn and M. E. Rose, Rev. Mod. Phys. **25**, 729 (1953).
[35] K. S. Krane and R. M. Steffen, Phys. Rev. C **2**, 724 (1970).
[36] C. J. Chiara, D. Weisshaar, R. V. F. Janssens, Y. Tsunoda, T. Otsuka, J. L. Harker, W. B. Walters, F. Recchia, M. Albers, M. Alcorta *et al.*, Phys. Rev. C **91**, 044309 (2015).
[37] B. A. Brown and W. D. M. Rae, MSU-NSCL Report (2007).
[38] A. F. Lisetskiy, B. A. Brown, M. Horoi, and H. Grawe, Phys. Rev. C **70**, 044314 (2004).
[39] M. Hasegawa, Y. Sun, K. Kaneko, and T. Mizusaki, Phys. Lett. B **617**, 150 (2005).
[40] B. Mukherjee, S. Muralithar, R. P. Singh, R. Kumar, K. Rani, R. K. Bhowmik, and S. C. Pancholi, Phys. Rev. C **64**, 024304 (2001).
[41] W. Nazarewicz, J. Dudek, R. Bengtsson, T. Bengtsson, and I. Ragnarsson, Nucl. Phys. A **435**, 397 (1985).
[42] W. Nazarewicz, M. A. Riley, and J. D. Garrett, Nucl. Phys. A **512**, 61 (1990).